

Probing Cytotoxicity of Gadolinium Hydroxide Nanostructures

Eva Hemmer,^{†,‡} Yvonne Kohl,^{†,§} Victoria Colquhoun,^{||} Hagen Thielecke,[§] Kohei Soga,[‡] and Sanjay Mathur^{*,†,⊥}

Department of Materials Science and Technology, Tokyo University of Science, 2641 Yamazaki, 278-8510 Chiba, Japan, Fraunhofer Institute for Biomedical Engineering, Ensheimer Strasse 48, 66386 St. Ingbert, Germany, Institute of Inorganic Chemistry, Technical University Dortmund, Otto-Hahn-Str. 6, 44227 Dortmund, Germany, and Institute of Inorganic Chemistry, University of Cologne, Greinstrasse 6, 50939 Cologne, Germany

Received: December 7, 2009; Revised Manuscript Received: February 11, 2010

Gadolinium hydroxide, Gd(OH)_3 , nanostructures were examined for their possible use in imaging and tracking of cells and tissues by investigating their cellular interactions and cytotoxic behaviors. For this purpose, Gd(OH)_3 nanorods (length, several hundred nanometers; diameter, $\sim 40 \text{ nm}$) and spherical nanoparticles (average diameter, $< 10 \text{ nm}$) were synthesized by solvothermal decomposition of gadolinium containing molecular precursors. After comprehensive characterization of material properties, human colon adenocarcinoma (Caco2) and human lung epithelial (A549) cells were incubated with Gd(OH)_3 nanostructures in concentrations up to $900 \mu\text{g/mL}$ to perform cytotoxicity assays (BrdU (5-bromo-2'-deoxyuridine), WST-1 (4-[3-(4-iodophenyl)-2-(4-nitrophenyl)-2H-5-tetrazolio]-1,3-benzol-disulfonate)) and living/dead staining. As observed in all in vitro assays, the investigated Gd(OH)_3 nanostructures do not induce any significant cytotoxic effect, making them promising candidates for a new class of contrast agents, which may overcome the limitations of organic stains such as photobleaching and single usage.

Introduction

The growing potential and interest in the application of engineered nanostructures for drug-delivery and other biomedical applications (e.g., coatings on implants, biomarkers and diagnostics) have enhanced the likelihood of nanobio interactions, which are difficult to predict due to lack of systematic studies and the diverse range of engineered nanomaterials that had become available in the past decade. Recent studies have shown the ability of artificially engineered nanostructures to transfer across biological barriers, which have triggered their applications in drug delivery and controlled release, as active surfaces in implants, and as biomarkers in cell-tracking or diagnostics studies.^{1–6} Luminescent inorganic materials possess high intensity and photostability, whereas the organic dyes used in current fluorescence-based bioimaging suffer from color fading resulting in temporal and limited use.⁷ Tunable optical properties of semiconductor nanoparticles (e.g., CdSe) have made them promising alternatives against recently used organic dyes;^{8–10} however, their intrinsic toxicity limits their applications. Alternative approaches to fabricate core–shell structures like CdSe/ZnS, with a biocompatible shell on luminescent quantum dots have been only marginally successful so far.¹¹ Further, the “on” and “off” switching of their luminescence emission, also known as flickering or blinking, is detrimental for their potential applications.¹² In this context, lanthanide (Ln)-based inorganic materials with their outstanding optical and magnetic properties are interesting alternatives for applications such as biomarkers,

sensors, and contrast agents in magnetic resonance imaging (MRI).^{13–18} With the exception of La^{3+} and Lu^{3+} , all trivalent lanthanide ions possess unpaired electrons resulting in paramagnetic behavior, among which gadolinium containing compounds are preferred as contrast agents in medical diagnostics due to the high magnetic moment of Gd ($7/2 \mu_B$).^{19,20} Burnett et al. chose Gd_2O_3 for MRI due to its selective liver-spleen clearance and paramagnetic properties.²¹ Already in 1980, gadolinium oxide was proposed as contrast material for computer tomography of the liver due to its excellent X-ray absorption properties and its high content of radiopaque metal.²² However, the concerns associated with the alteration of biophysicochemical properties upon the interaction of cells with inorganic particles and vice versa are still eligible. Recent studies investigated the role of particle-induced reactive oxygen species (ROS) as well as oxidative stress in nanoparticle toxicity^{23,24} and a hierarchical oxidative stress model was formulated by Nel et al. to classify potentially hazardous or safe nanoparticles.²⁵ Nevertheless, there is still a demand of improved understanding of nanobio interactions,^{26–29} which necessitates besides the development of nanostructures with suitable optical and magnetic properties and investigation of their biocompatibility and cytotoxicity as well as chemical stability in physiological media.

Increasing interest in multifunctional nanomaterials for biomedical applications^{30,31} has resulted in the development of risk management protocols³² and numerous studies addressing the toxicology of nanostructures.^{33–35} These studies have shown the in vivo uptake of nanostructures via respiratory tract, gastrointestinal tract, and skin. Increased cytotoxicity may be expected for ultrasmall particles due to potential interactions with intracellular proteins, organelles and DNA after crossing the cell membrane. Recent cytotoxic studies include investigation of metal oxide nanoparticles like TiO_2 ,^{36,37} ZrO_2 , Al_2O_3 , and Fe_2O_3 ,³⁵ carbon-based structures like carbon black²⁴ and

* Correspondence: sanjay.mathur@uni-koeln.de, Phone: +49-221-470-4107, Fax: +49-221-470-4899.

[†] Contributed equally to this work.

[‡] Tokyo University of Science.

[§] Fraunhofer Institute for Biomedical Engineering.

^{||} Technical University Dortmund.

[⊥] University of Cologne.

carbon nanotubes³⁸ as well as metals like gold,³⁹ silver, or aluminum nanoparticles.⁴⁰ Among rare earth containing compounds, gadolinium-based MRI contrast agents^{41,42} and GdCl_3 ⁴³ have been examined, while only a few reports about lanthanide oxides and hydroxides have been published.^{44,45} Besides size, morphology plays an important role in the cytotoxicity of nanomaterials. For instance, one-dimensional structures like nanowires or nanorods with several 100 nm length and a few tens of nanometers in diameter may interact with cells in a different manner than isotropic nanoparticles. While particles may cross the cell membrane if their size is small enough, nanorods and wires are at least in one dimension (length) too large to be completely taken up by the cell. Therefore, different cytotoxic effects could be expected concerning different shapes of the nanostructures.

Our interest lies in the preparation of lanthanide containing nanomaterials with respect to future application in biomedicine or diagnostics and to investigate their cytotoxic behavior, when they interact in vitro with the living cells. Different nanorods and nanoparticles prepared by solvothermal decomposition of gadolinium precursors were investigated to elucidate the morphology–cytotoxicity relationship.

Experimental Methods

Precursor Synthesis. For gadolinium oleate ($\text{Gd}(\text{oleate})_3$) synthesis, 10 mmol of $\text{GdCl}_3 \cdot 6\text{H}_2\text{O}$ and 30 mmol of sodium oleate were stirred in a mixture of hexane (35 mL), ethanol (20 mL), and water (15 mL) at 70 °C for 4 h. To complete the reaction, the solution was stirred at room temperature for a further 14 h (yield: 90%).⁴⁶ After washing with an ethanol–water mixture (1:1), an air and moisture stable product was obtained as a colorless waxy solid. The good agreement of the results of elemental analysis with calculated carbon and hydrogen content and the characteristic metal–carboxylate stretches in the FT-IR (Fourier transform infrared) spectrum at 1650–1510 cm^{-1} confirmed the formation of the desired compound. Anal. Calcd: C, 64.75; H, 9.96. Found: C, 62.76; H, 10.12.

Due to the moisture sensitive nature of starting materials, synthesis of gadolinium *tert*-butoxide, $[\text{Gd}_3(\text{O}'\text{Bu})_9(\text{HO}'\text{Bu})_2]$, was performed using modified Schlenk techniques adapting the synthesis route published by Bradley et al.⁴⁷ Solvents were dried before use by standard procedures and stored over sodium or molecular sieves. In a typical reaction, 0.9 g (1.4 mmol) of $\text{Gd}\{\text{N}(\text{SiMe}_3)_2\}_3$ ⁴⁸ was solved in 20 mL of hexane and 1 mL of THF and the solution was cooled to –70 °C followed by the addition of 10 mL of *tert*-butanol. The mixture was stirred at room temperature for 24 h. After the evaporation of solvent and recrystallization from 15 mL of toluene followed at 4 °C, colorless crystals were obtained (yield: 60%). Anal. Calcd: C, 41.35; H, 7.97. Found: C, 41.81; H, 7.87. Experimental details of the single crystal X-ray diffraction analysis of $[\text{Gd}_3(\text{O}'\text{Bu})_9(\text{HO}'\text{Bu})_2]$ are listed in Table 1.

Material Synthesis. For $\text{Gd}(\text{OH})_3$ nanorod preparation 200 mg of gadolinium oleate complex was dissolved in 20 mL of hexane and the solution was transferred into a Teflon inliner ($V = 50$ mL) followed by controlled hydrolysis using 1 mL of an aqueous potassium hydroxide solution ($c = 1.87$ mol/L). $\text{Gd}(\text{OH})_3$ nanoparticles were obtained by solvothermal treatment of a solution of 150 mg of gadolinium *tert*-butoxide in 10 mL of toluene that was previously activated by slow addition of a mixture of 0.5 mL of H_2O in 25 mL of toluene. For the solvothermal treatment, stainless steel DAB-2 autoclaves (Berg-hof Products + Instruments GmbH) were used. The process temperature was maintained at 250 °C, and the reaction time

TABLE 1: Experimental Details of the Single Crystal X-ray Diffraction Analysis of $[\text{Gd}_3(\text{O}'\text{Bu})_9(\text{HO}'\text{Bu})_2]$

empirical formula	$\text{C}_{109}\text{H}_{222}\text{Gd}_6\text{O}_{22}$		
chemical formula	$[\text{Gd}_3(\text{O}'\text{Bu})_9(\text{HO}'\text{Bu})_2(\text{C}_2\text{H}_8)_2]$		
formula weight	2828.37 g mol ^{−1}		
temperature	99(2) K		
radiation, λ	MoK α , 0.71073 Å		
crystal system	monoclinic		
space group	$P2_1/n$		
unit cell dimensions	$a = 14.6356(6)$ Å	$\alpha = 90.00^\circ$	
	$b = 23.5944(11)$ Å	$\beta = 106.868^\circ$	
	$c = 19.3545(8)$ Å	$\gamma = 90.00^\circ$	
volume	6395.9(5) Å ³		
Z	2		
calculated density	1.469 Mg m ^{−3}		
absorption coefficient	3.124 mm ^{−1}		
$F(000)$	2872		
θ range for collection	1.40 to 26.08°		
index range	$-18 \leq h \leq 18$		
	$-29 \leq k \leq 29$		
	$-23 \leq l \leq 23$		
no. of reflections collected	12639		
refinement method	full-matrix least-squares on F^2		
no. of data/parameters/restraints	12639/64/682		
goodness of fit on F^2	1.094		
final R indices [$I > 2\sigma(I)$]	$R_1 = 0.0180$, $wR_2 = 0.0392$		
R indices (all data)	$R_1 = 0.0219$, $wR_2 = 0.0421$		
max/min residual electron density	+1.810/−1.198 e Å ^{−3}		

was 24 h. The atogenous pressure was estimated with the aid of the ideal gas law and Peng–Robinson equation.^{49,50} When decomposition took place in 20 mL of hexane, the estimated pressure was approximately 50 bar whereas use of 35 mL of toluene led to an approximate value of 150 bar. After cooling to room temperature, the obtained precipitates were washed several times with methanol and ethanol, collected by centrifugation and dried under ambient conditions.

Material Characterization. Elemental analysis was achieved with a Vario Micro Cube (Elementar Analysen Systeme, Hanau). Infrared (IR) absorption spectra of gadolinium oleate precursor were recorded with a Bruker spectrometer Vektor 22. The decomposition behavior of the oleate complex was investigated by differential thermogravimetry/differential thermoanalysis studies in 60 sccm nitrogen using a TGA 1500 by Bähr with a heating rate of 10 K/min. The crystal data of $[\text{Gd}_3(\text{O}'\text{Bu})_9(\text{HO}'\text{Bu})_2]$ were collected on a Bruker X8APEX diffractometer with a CCD area detector and multilayer mirror monochromated Mo K α radiation. The structure was solved using direct methods, refined with the Shelx software package,⁵¹ and expanded using Fourier techniques. All non-hydrogen atoms were refined anisotropically. Hydrogen atoms were assigned to idealized positions and were included in structure factor calculations. Powder X-ray diffraction (XRD) patterns were recorded on a Philips PW 1710 diffractometer (45 kV, 30 mA; step size, 0.02°) and indexed with the aid of the program X'Pert HighScore (Philips Analytical B. V., Almelo, Netherlands). Transmission electron microscopy (TEM) was performed on a CM200 transmission electron microscope (Philips). Scanning electron micrographs (SEM) of cells incubated with $\text{Gd}(\text{OH})_3$ nanorods were recorded using a scanning electron microscope JSM-7000F. For FT-IR spectroscopy of the nanorods incubated in pure medium (DMEM with fetal calf serum (FCS), RPMI with FCS and L-glutamine) samples were mixed with KBr and the transmission was recorded under vacuum conditions using a JASCO FT/IR-6200 spectrometer. Emission spectrum of the europium-doped sample

was recorded at room temperature using a RF-5000 spectrophotometer by Shimadzu-Seisakusho.

In Vitro Cytotoxicity Tests. (i) **Pretreatment of the Nanostructures for Cytotoxicity Tests.** The as-prepared nanomaterials were sterilized by UV–Vis (ultraviolet–visible) light for 6 h. Cell culture medium, supplemented with FCS (fetal calf serum), was used to prepare the stock solutions. To break larger agglomerates, each suspension was sonicated (Ultrasonic Cleaner) for 15 min prior to exposure to the cells.

(ii) **Cell Culture and Exposure to Nanomaterials.** Two different cell culture systems were used for the in vitro study of the nanostructure cytotoxicity: human lung epithelial cells (A549, purchased from American Type Culture Collection, Manassas, VA) and human colon epithelial cells (Caco2, purchased from American Type Culture Collection, Manassas, VA). A549 cells were maintained in RPMI 1640 medium (Invitrogen, Carlsbad, CA), supplemented with 10% FCS, 100 U/mL penicillin and 100 µg/mL streptomycin. Caco2 cells were cultured in DMEM/F-12 (1:1) (Invitrogen), supplemented with 20% FCS, 100 U/mL penicillin, and 100 µg/mL streptomycin. All cell culture systems were cultured at 37 °C, 5% CO₂ and 95% saturated atmospheric humidity. Nanorods were added to the cell culture medium to give a final concentration in the range from 50 to 250 µg/mL. The final concentrations of nanoparticles ranged from 25 to 900 µg/mL. A total of 1.0 × 10⁴ cells were placed in each well of a 96-well plate and cultured in 100 µL of cell culture medium, containing 10% FCS, for 24 h at 37 °C. The next day, 100 µL of the nanostructure suspension was added to the cell culture plate for incubation, and the cells were incubated for 4 and 24 h. The control cells received only cell culture medium (with supplements) without gadolinium hydroxide. Each experiment included a positive control which was Triton X at a concentration of 1%. After the nanostructure incubation, viability of the cells was evaluated by cytotoxicity assays.

(iii) **Cytotoxicity Assays. WST-1 Assay.** To measure the metabolic function of the exposed cells, the WST-1 based colometric assay was employed. The assay is based on the cleavage of stable tetrazolium salt WST-1 (4-[3-(4-iodophenyl)-2-(4-nitrophenyl)-2H-5-tetrazolio]-1,3-benzol-disulfonate) to a soluble formazan by a complex cellular mechanism that occurs primarily at the cell surface. The amount of formazan dye formed directly correlates to the number of metabolically active cells in the culture. After incubation according to manufacturer's instructions with appropriate controls, the formed formazan dye is quantified with a scanning multiwell spectrophotometer (ELISA reader). The measured absorbance directly correlates to the number of viable cells. The net absorption change taken from the wells of untreated cultured cells was used as the 100% viability value (negative control).

(iv) **BrdU Assay.** The detection of the proliferation rate of the exposed cells was performed using the BrdU assay kit by Roche Diagnostics (Mannheim, Germany). This colorimetric immunoassay is based on the measurement of BrdU (5-bromo-2'-deoxyuridine) incorporation during DNA synthesis. The reaction product is quantified by measuring the absorbance using a scanning multiwell spectrophotometer (ELISA reader).

(v) **Living/Dead Staining.** To visualize viable and dead cells after the incubation with Gd(OH)₃ nanostructures, a dye mixture of fluorescein diacetate (FD) and propidium iodide (PI) was employed to stain the cells. After incubation and staining for 15 s, cells were washed with PBS buffer to remove the excess dye molecules. Before observation in inverse fluorescence microscope (Observer Z1, Zeiss), cells were covered with PBS

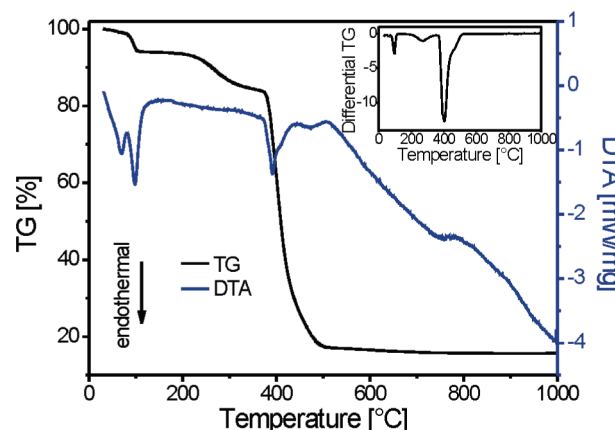


Figure 1. TG-DTA analysis of Gd(oleat)₃.

buffer. Living cells showed a green fluorescent signal, while dead cells were stained by the red fluorescent PI dye.

(vi) **Statistical Analysis.** Experiments were replicated three independent times and data are presented as mean ± SD (standard deviation). For the in vitro studies, each stock solution was diluted serially to yield the different concentrations. Each experimental value was compared to the corresponding control value for each time point. Statistical significance versus control (pure cell culture media) was established as *p* < 0.05. Statistical tests were performed with OriginPro 7.5G software. The analysis of the percentage of survival cells and dead cells after the living/dead staining was performed with the aid of the image analysis software Cell Profiler 1.0.5122. For the cell tests, 10 000 cells/well with a doubling time of 24 h were seeded. No confluence was achieved after 24 h.

Results and Discussion

Synthesis and Characterization of Gadolinium Containing Precursors and Gd(OH)₃ Nanostructures. Metal oleate complexes are suitable starting compounds for the synthesis of nanoscale metals, metal oxides, or metal sulfides, as shown by Hyeon et al. and Bronstein et al.^{46,52} Mahajan et al. reported the decomposition of lanthanide oleates in high boiling solvents resulting in Ln₂O₃ nanocrystals (Ln = Gd, Tb, Eu).⁵³ Gadolinium hydroxide nanorods were produced by solvothermal decomposition of gadolinium oleate synthesized by salt elimination reaction of gadolinium chloride hexahydrate with sodium oleate in a mixture of hexane, ethanol and water following the procedure described by T. Hyeon et al.⁴⁶ Thermogravimetric analysis (TG-DTA) of the gadolinium oleate complex (Figure 1) illustrated that the thermal decomposition of Gd(oleate)₃ proceeds in a temperature range 370–510 °C under ambient pressure. At 392 °C a strong endothermal peak is observed in the DTA curve that corresponds to the main weight loss of 69% indicating the formation of Gd(OH)₃. This observation corresponds to the data reported by Mahajan et al.⁵³

Gd(OH)₃ nanostructures were synthesized by solvothermal treatment (250 °C, 24 h) of (i) gadolinium oleate complex in hexane and aqueous KOH and (ii) gadolinium alkoxide precursor in toluene and water. Gadolinium *tert*-butoxide (Figure 2) was obtained by alcoholysis of gadolinium trisilylamide with *tert*-butanol as described in literature for analogous lanthanide *tert*-butoxides (Ln = Y, La, Nd, Dy).^{47,54–56} It acts as a molecular source for both Gd and O and allows a controlled synthesis of gadolinium hydroxide nanostructures.

Irrespective of the chosen solvothermal treatment (eq 1), both oleate and alkoxide precursor resulted in the formation of the

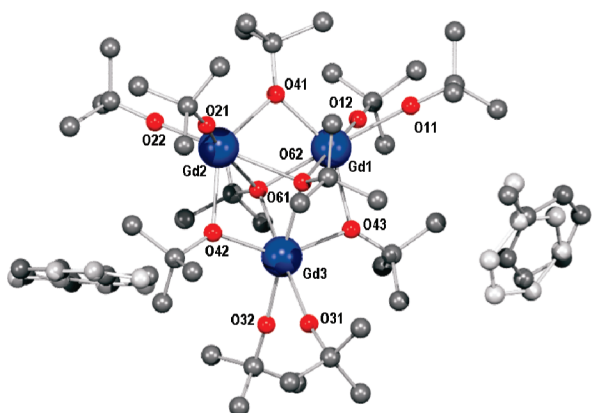


Figure 2. Molecular structure of $[Gd_3(O'Bu)_9(HO'Bu)_2]$. Hydrogen atoms are omitted for clarity. Selected bond lengths and angles: Gd1–O41, 2.2804(15) Å; Gd1–O43, 2.3313(16) Å; Gd1–O61, 2.3610(15) Å; Gd1–O62, 2.4139(15) Å; Gd1–O11, 2.5567(16) Å; Gd1–O12, 2.1223(16) Å; Gd1–O41–Gd2, 38.51(4)°; O41–Gd1–O43, 143.54(5)°; O11–Gd1–O12, 72.53(6)°.

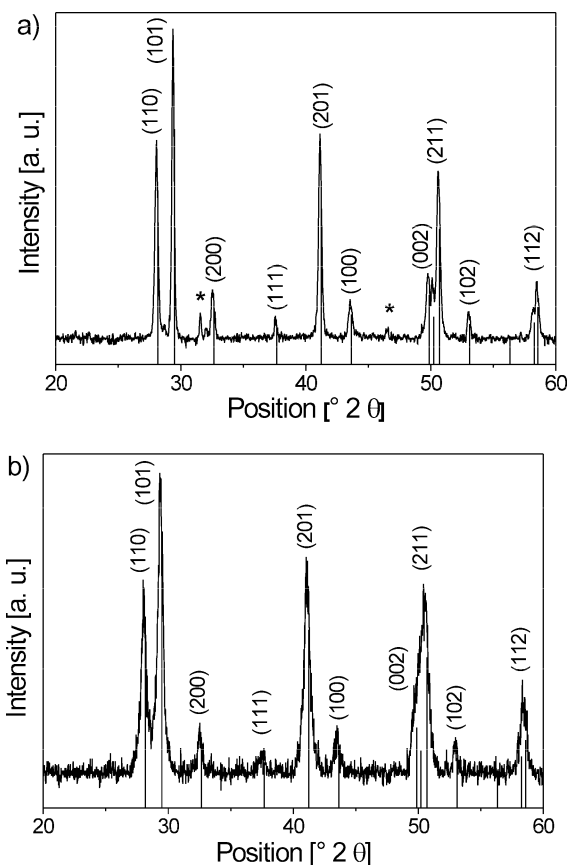
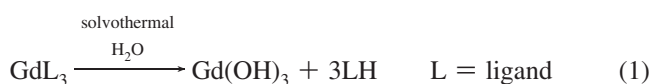


Figure 3. X-ray diffraction patterns of $Gd(OH)_3$ powders obtained from solvothermal treatment of (a) $Gd(\text{oleat})_3$ and (b) $[Gd_3(O'Bu)_9(HO'Bu)_2]$. Reference file: $Gd(OH)_3$, [PDF 83-2037].

hydroxide phase, which was confirmed by the powder X-ray diffraction analysis (Figure 3).



When $Gd(\text{oleate})_3$ was used, the obtained pattern showed two additional peaks of low intensity at 31.5° and 46.5°

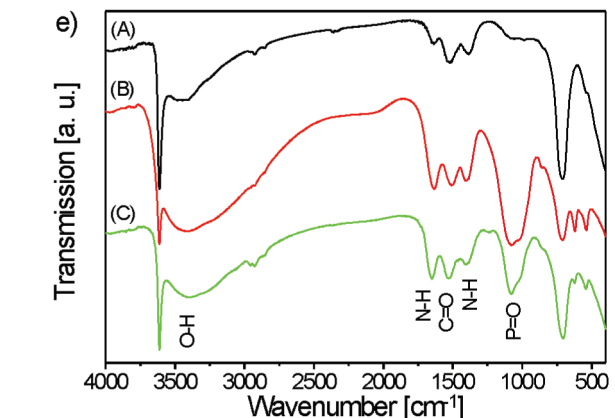
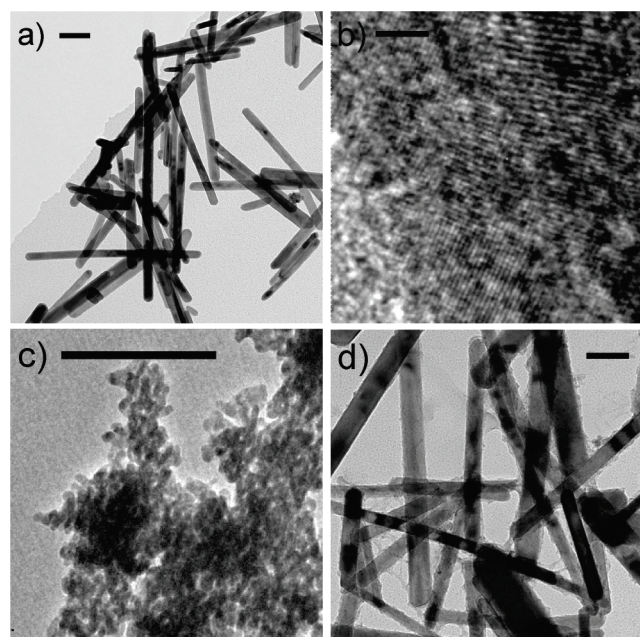


Figure 4. TEM images of $Gd(OH)_3$ nanostructures obtained by solvothermal treatment of (a, b) $Gd(\text{oleate})_3$ and (c) $[Gd_3(O'Bu)_9(HO'Bu)_2]$, respectively. (d) $Gd(OH)_3$ nanorods after 24 h in cell culture media. (e) FT-IR spectra of as-prepared (A), in DMEM (B) and RPMI (C) incubated $Gd(OH)_3$ nanorods. Scale bar: 100 nm (a, c, d) and 3 nm (b).

(Figure 3a), which were assigned to the gadolinium silicate phase $Gd_{4.67}(SiO_4)_3O$ ([PDF-72-2070]) and are possibly caused by silicon contamination present in the starting materials.

TEM micrographs of powders obtained from gadolinium oleate precursor (Figure 4a) revealed uniform nanorods with an average diameter of ca. 30–40 nm and an aspect ratio between 15 and 20. High resolution TEM image confirmed the high crystallinity of the material (Figure 4b), with observed interplanar spacing of (110) plane (3.2 \AA) corresponding to those expected for $Gd(OH)_3$ ($d(110) = 3.16 \text{ \AA}$).

Gadolinium hydroxide crystallizes in the hexagonal lattice ($a = 6.3290 \text{ \AA}$, $b = 6.3290 \text{ \AA}$, $c = 3.6310 \text{ \AA}$) where the anisotropic growth is governed by crystal chemistry and chemical potential of $Gd(OH)_3$ in solution.^{57–60} Consequently, no templates are required to obtain elongated structures. Formation of elongated nanostructures is a pronounced tendency in lighter lanthanide elements, as shown by Wang and co-workers.⁵⁸ A high chemical potential tunable by the pH value of the reaction mixture, supported one-dimensional growth (Figure 4a), which also suggested the possible modification of

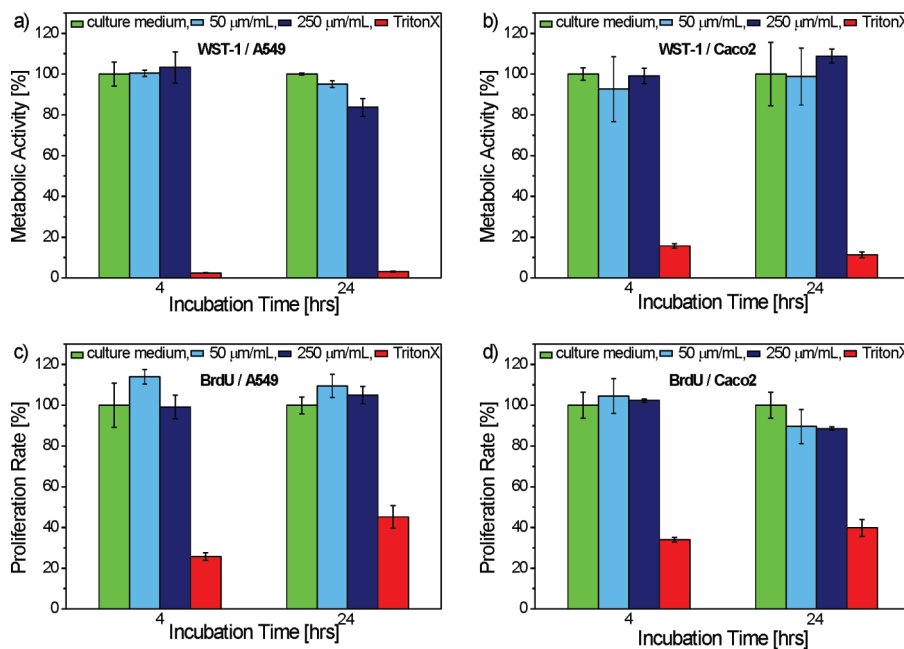


Figure 5. Metabolic activity of (a) A549 and (b) Caco2 cells and proliferation rate of (c) A549 and (d) Caco2 cells incubated with $\text{Gd}(\text{OH})_3$ nanorods.

morphology upon variation in the pH of the reaction mixture. This assumption was confirmed by TEM-investigations of the powders obtained by solvothermal treatment of gadolinium *tert*-butoxide, which produced nanoscale particles (Figure 4c) with the average diameter being less than 10 nm. The stability of gadolinium hydroxide nanostructures in cell culture media was tested by dispersing and storing them in RPMI media. TEM investigations after 24 h revealed no substantial changes in the morphological features under cell test conditions (Figure 4d).

Changes in surface chemistry of the $\text{Gd}(\text{OH})_3$ nanorods during incubation in both cell culture media DMEM and RPMI were monitored by transmittance FT-IR spectroscopy (Figure 4e), which showed, when compared to as-prepared nanorods (A), an additional peak at 1080 cm^{-1} , indicating the presence of $\text{P}=\text{O}$ groups. Other peaks in as-synthesized and incubated nanorods can be attributed to the characteristic metal–oxygen vibrations ($710\text{--}540\text{ cm}^{-1}$) and hydroxyl stretches ($3700\text{--}3200\text{ cm}^{-1}$) of the metal attached $-\text{OH}$ groups and hydrogen bonding among surface-adsorbed water molecules. The observed increase in intensity of the peak ranging from 1700 to 1350 cm^{-1} is possibly due to adsorption of amino acids present in the cell culture media on the surface of the nanorods. Similar findings were reported by Tkaczyk et al. who investigated formation of chromium(III) complexes in simulated physiological fluids DMEM and RPMI.⁶¹ The higher peak intensity due to $\text{P}=\text{O}$ groups after incubation in RPMI can be explained by the higher concentration of PO_4 in RPMI (800 mg/mL Na_2HPO_4) compared to DMEM (134 mg/mL $\text{Na}_2\text{HPO}_4 \cdot 7\text{H}_2\text{O}$, 62.5 mg/mL $\text{NaH}_2\text{PO}_4 \cdot \text{H}_2\text{O}$).

One of the reasons for the rather low cytotoxicity of $\text{Gd}(\text{OH})_3$ nanostructures can be attributed to the *in situ* surface modification of $\text{Gd}(\text{OH})_3$ during incubation with PO_4 groups and amino acids. The lower toxicity of Cr(III) due to the reaction of the metal ions with PO_4 groups was recently reported.⁶¹ Interaction between nanomaterials and biological molecules, e.g., proteins, was investigated by several groups and is promising with regard to applications in nanobiotechnology.⁶² However, interaction between inorganic nanostructures and biomolecules in physiological fluid phases like cell culture media used in cytotoxicity tests can also induce depletion of nutrient in the media resulting

in an *indirect* cytotoxicity, as reported by Gua et al. for carbon nanotubes adsorbing amino acids and vitamins from RPMI cell culture media.⁶³

Cytotoxicity of $\text{Gd}(\text{OH})_3$ Nanostructures. (i) **Cytotoxicity of $\text{Gd}(\text{OH})_3$ Nanorods.** The metabolic activity of the two chosen cell lines (human colon adenocarcinoma cells (Caco2) and human lung epithelial cells (A549)), after their incubation with nanorods suspension (50 and 250 µg/mL), was determined via the WST-1 assay. The cytotoxicity was analyzed after two exposure time periods (4 and 24 h). Compared to the negative control (cell culture medium), no significant decrease of the metabolic activity of A549 cells was observed at the tested nanorod concentrations (50 and 250 µg/mL) (Figure 5a). Also, no time-dependent effect was detected at a concentration of 50 µg/mL, as evident in Figure 5a. Even a higher concentration of 250 µg/mL $\text{Gd}(\text{OH})_3$ induced no significant decrease of the metabolic activity compared to the negative control. When compared to the result obtained at a nanorod concentration of 50 µg/mL, 250 µg/mL induced a decrease of the metabolic activity to 82% after 24 h of incubation.

After the incubation of different nanorod concentrations with Caco2 cells, no decrease in metabolic activity or any cytotoxic influence was detected using the WST-1 assay (Figure 5b). The metabolic activity reached 109% at the highest tested concentration of $\text{Gd}(\text{OH})_3$ nanorods (250 µg/mL, 24 h).

The effect of the $\text{Gd}(\text{OH})_3$ nanorods on the proliferation rate of the used cell lines was determined via the BrdU assay. The results (Figure 5c,d) for both A549 and Caco2 cells showed no dose-dependent cytotoxicity of $\text{Gd}(\text{OH})_3$ nanorods. At the highest tested concentration (250 µg/mL, 24 h) the cell proliferation rates were found to be 105% for A549 cells (Figure 5c) and 89% for Caco2 cells (Figure 5d), respectively.

Furthermore, the living/dead staining tests performed on cells incubated for 24 h (Figure 6) support the results obtained from cytotoxicity assay. Performing a living/dead staining under the same incubation conditions (250 µg/mL) showed that approximately 20% of the cells were identified as dead cells (Figure 6a) which is in good agreement with the WST-1 assay, whereas no decrease in viability of A549 cells was detected in

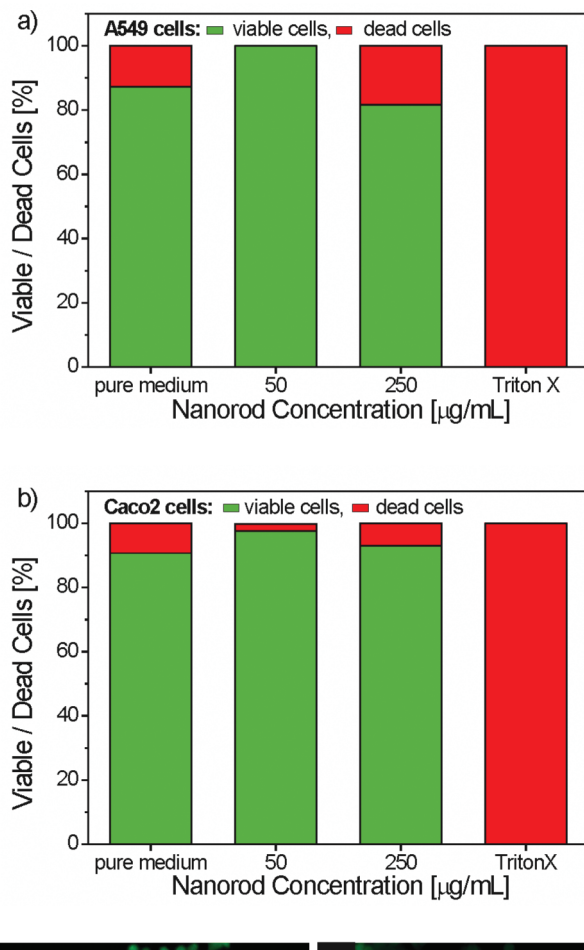


Figure 6. Analysis of the percentage of viable and dead A549 (a) and Caco2 (b) cells incubated with $\text{Gd}(\text{OH})_3$ nanorods and fluorescence images of A549 (c) and Caco2 (d) cells after fluorescein diacetate staining ($t = 24 \text{ h}$, $c = 250 \mu\text{g/mL}$). Scale bar: 50 nm.

the case of incubation performed with 50 $\mu\text{g/mL}$ $\text{Gd}(\text{OH})_3$ nanorods (Figure 5a). As obvious from the determined percentage of living and dead Caco2 cells incubated for 24 h with different concentrations of $\text{Gd}(\text{OH})_3$ nanorods (Figure 6b), there is no significant change in the viability of the investigated cell population compared to the negative control. The fluorescence microscopy images taken from the respective A549 (Figure 6c) and Caco2 (Figure 6d) cells confirm the high percentage of living cells.

The living/dead staining reveals the percentage of viable and dead cells; however, it does not provide any insight on the interaction between the nanostructures and the cells. Information on cellular uptake or interaction of the nanorods on the surface of the cell membrane, active movement of the cell toward areas of high nanorod concentration or, in contrast, avoidance of the nanostructures, was gathered by SEM of A549 cells incubated with $\text{Gd}(\text{OH})_3$ nanorods (Figure 7), which displayed nanorod agglomerates on the surface of the cell membrane. Hereby, no change of the characteristic morphology of the A549 cells was induced by incubation of 250 $\mu\text{g/mL}$ nanorods for 24 h.

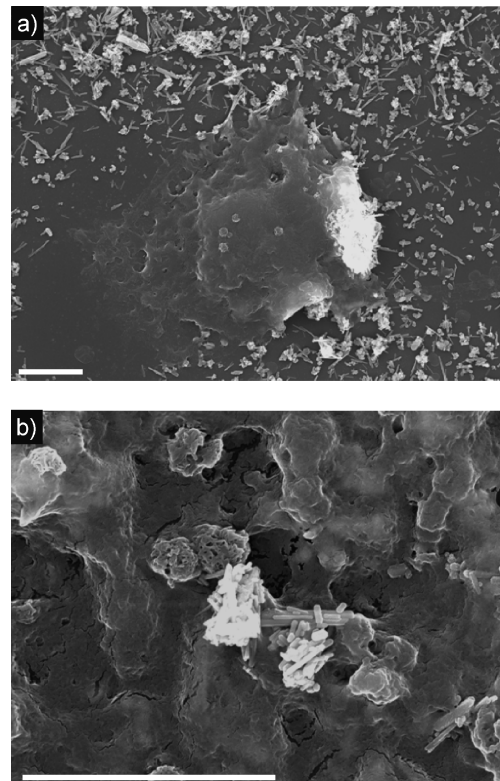


Figure 7. Scanning electron micrograph of A549 cells incubated with $\text{Gd}(\text{OH})_3$ nanorods ($t = 24 \text{ h}$, $c = 250 \mu\text{g/mL}$). (a) Overview of an A549 cell and (b) $\text{Gd}(\text{OH})_3$ nanorod agglomerations on the cell's membrane surface. Scale bar: 3 μm .

(ii) Effect of Nanostructure Morphology on Cytotoxicity. $\text{Gd}(\text{OH})_3$ nanoparticles with a diameter of 10 nm were analyzed for their cytotoxic activity via WST-1 assay. Similar to the observed mode for nanorods, no significant decrease of the metabolic activity of A549 cells was observed after 4 and 24 h (Figures 5 and 8a). At the highest tested concentration (900 $\mu\text{g/mL}$) the cell viability reached an average value of 100%. $\text{Gd}(\text{OH})_3$ nanorods treated identically did not induce any significant increase of the metabolic activity after the tested incubation times (4 and 24 h, Figure 8b), which shows that in the case of $\text{Gd}(\text{OH})_3$ nanostructures, morphology apparently does not contribute toward cytotoxic behavior.

A morphology-induced effect on the cytotoxic behavior of $\text{Gd}(\text{OH})_3$ nanorods was anticipated due to their mechanical strength and potential to perforate the cell membrane, while nanoparticles can translocate through cell membrane owing to their tiny dimensions. Furthermore, investigations of various nanoparticles by other groups implicate a correlation of a potential toxicity with the specific surface area of the nanostructures.³⁵ Yang et al. investigated the cytotoxicity of carbon black, carbon nanotubes, SiO_2 , and ZnO and suggested a correlation between the chemical composition, the surface properties, and the reactive oxidative stress generation, while genotoxicity is primarily influenced by the shape of the nanostructure revealing a higher toxicity for carbon nanotubes than for ZnO nanoparticles.²⁴

The rather low cytotoxicity of $\text{Gd}(\text{OH})_3$ nanostructures can be attributed to the clustering of the nanostructures to form agglomerates, which inhibits cytotoxic influence. The difficulty of preparing dispersed single nanoparticles is well-known and usually surface modification is required to separate each particle by either steric or electrostatic repulsion.^{64,65} However, in this study unmodified $\text{Gd}(\text{OH})_3$ nanostructures (nanoparticles of less

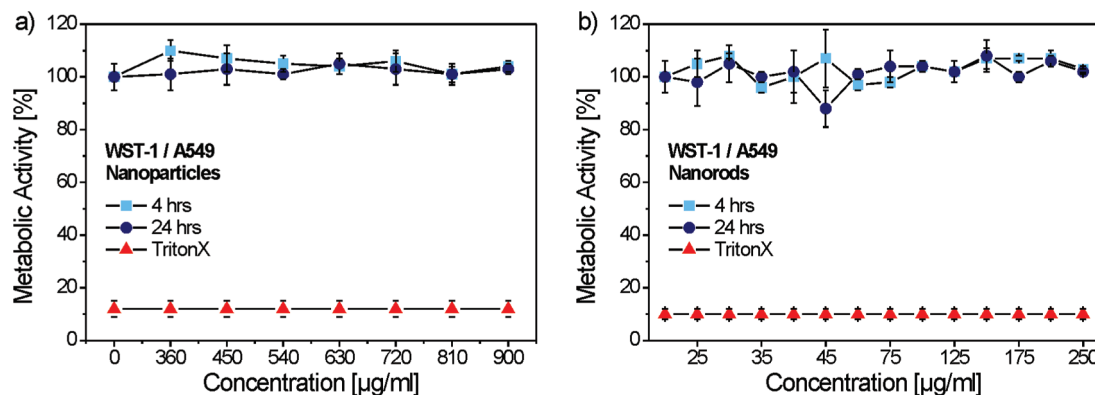


Figure 8. Metabolic activity of A549 cells after incubation with (a) $\text{Gd}(\text{OH})_3$ nanoparticles and (b) $\text{Gd}(\text{OH})_3$ nanorods.

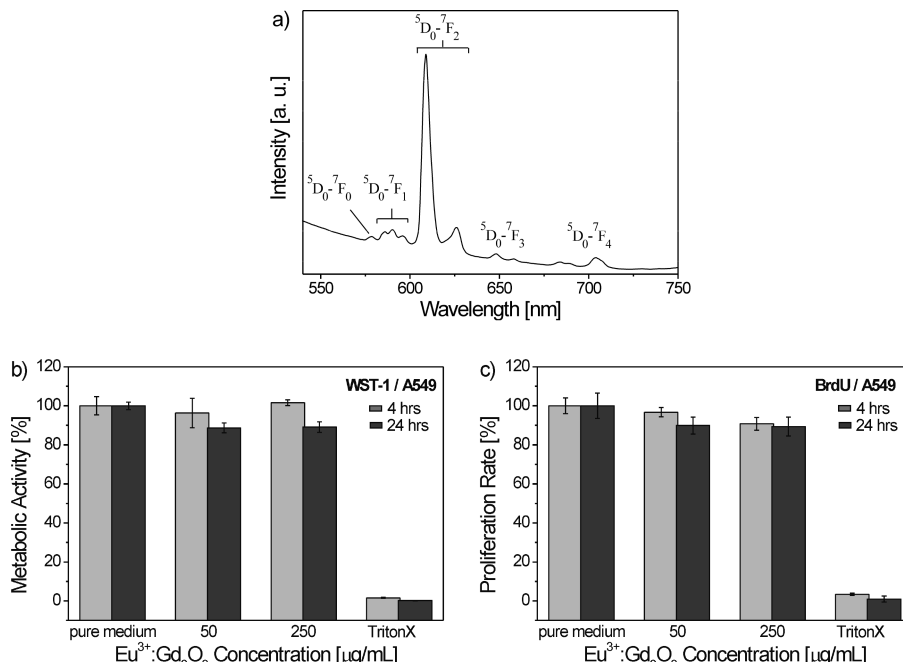


Figure 9. (a) Room temperature emission spectrum of annealed $\text{Eu}^{3+}:\text{Gd}_2\text{O}_3$ nanostructures ($\Delta T = 1100^\circ\text{C}$, $\lambda_{\text{ex}} = 393.3\text{ nm}$). (b) Metabolic activity (WST-1) and (c) proliferation rate (BrdU) of A549 cells.

than 10 nm in diameter and nanorods with a length of several hundreds of nanometers and a diameter of 40 nm) were investigated. A similar cell activity for both morphologies supports the suggested suppression of cytotoxicity through agglomeration.

(iii) **Optical and Cytotoxic Properties of $\text{Eu}^{3+}:\text{Gd}_2\text{O}_3$ Nanostructures.** With regard to future applications as biomarkers, nanostructures showing photoluminescence are required. In this context, as-prepared nanorods were doped with Eu³⁺ ions followed by an annealing step to obtain OH⁻-free, crystalline Eu³⁺:Gd₂O₃ nanostructures.⁶⁶ Gadolinium oxide is a well-known host material for doping with europium ions and Eu³⁺:Gd₂O₃ nanoparticles show a high potential for biomedical applications.⁶⁷ Investigation of the optical properties of the obtained powders by photoluminescence spectroscopy exhibited the characteristic emission spectrum corresponding to Eu³⁺ f-f transitions ($^5\text{D}_0 \rightarrow ^7\text{F}_J$, $J = 0, 1, 2, 3, 4$) with a maximum peak in the red range of the visible spectrum at 610 nm (Figure 9a).

As observed by WST-1 and BrdU assay (Figure 9b,c), incubation of Eu³⁺:Gd₂O₃ did not show any inhibitory effect on viability of A549 cells. No significant decrease of the metabolic activity was observed until the highest tested concentration of Eu³⁺:Gd₂O₃ nanorods (250 $\mu\text{g}/\text{mL}$). Cell prolifera-

tion of A549 cells incubated with 250 $\mu\text{g}/\text{mL}$ Eu³⁺:Gd₂O₃ did not significantly decrease. As also evident from WST-1 and BrdU assay, no time-dependent effect was detected. Our results indicate that the Eu³⁺-doped Gd₂O₃ can be used as biomaterials in medical applications due to Ln 4f intratransition and low cytotoxicity toward the cells.

Conclusion

The solvothermal decomposition of $\text{Gd}(\text{oleate})_3$ and $[\text{Gd}_3(\text{O}^{\prime}\text{Bu})_9(\text{HO}^{\prime}\text{Bu})_{11}]$ led to crystalline $\text{Gd}(\text{OH})_3$ nanorods and nanoparticles, respectively. Cytotoxic tests on Caco2 and A549 cells showed no potential inhibitory effects of the prepared nanostructures on cellular functions. In this study, neither nanorods nor nanoparticles exhibited any pronounced cytotoxic effect even at the highest tested concentrations. One reason for the absence of any morphology-induced cytotoxic effect is attributed to the agglomeration of the as-prepared nanoparticles to clusters that are too large to penetrate the cell membrane and therefore to interrupt biochemical pathways inside the cell. Further, hydrophilic attraction between the hydroxide groups present on the surface of the investigated $\text{Gd}(\text{OH})_3$ nanostructures and aqueous cell media may result in biocompatibility as

well as the *in situ* surface modification, for example, phosphate groups during incubation, as observed in the IR spectra. Surface modification to (i) prevent particle agglomeration and (ii) enable cell specific targeting, which is an important step on the way to understanding biochemical reactions at the nanoparticle–liquid interface during cell incubation, are underway. Preliminary experiments with europium-doped gadolinium oxide nanostructures indicate the investigated powders to be biocompatible, which makes gadolinium containing inorganic nanostructures to be a promising alternative to recently used contrast agents and fluorescent markers.

Acknowledgment. We thank Dr. H. Shen for SEM and TEM characterization and Dr. K. Radacki for X-ray single crystal analysis. Financial support was granted by the German Science Foundation (DFG) in the frame of the Schwerpunktprogramm SPP-1166 and the European Commission within the FP-7 Program (NANOMMUNE).

References and Notes

- (1) Wagner, V.; Dullaart, A.; Bock, A.-K.; Zweck, A. *Nat. Biotechnol.* **2006**, *24*, 1211–1217.
- (2) Resnik, D. B.; Tinkle, S. S. *Nanomedicine* **2007**, *2*, 345–350.
- (3) Salata, O. V. *J. Nanobiotechnol.* **2004**, *2*, 6 pp.
- (4) Doat, A.; Fanjul, M.; Pellé, F.; Hollande, E.; Lebugle, A. *Biomaterials* **2003**, *24*, 3365–3371.
- (5) Park, J.-A.; Reddy, P. A. N.; Kim, H.-K.; Kim, I.-S.; Kim, G.-C.; Chang, Y.; Kim, T.-J. *Bioorg. Med. Chem. Lett.* **2008**, *18*, 6135–6137.
- (6) Hifumi, H.; Yamaoka, S.; Tamimoto, A.; Citterio, D.; Suzuki, K. *J. Am. Chem. Soc.* **2006**, *128*, 15090–15091.
- (7) Shamer, N. C.; Lin, M. Z.; McKeown, M. R.; Steinbach, P. A.; Hazelwood, K. L.; Davidson, M. W.; Tsien, R. Y. *Nature Methods* **2008**, *5*, 545–551.
- (8) Bruchez, M., Jr.; Moronne, M.; Gin, P.; Weiss, S.; Alivisatos, A. P. *Science* **1998**, *281*, 2013–2016.
- (9) Chan, W. C. W.; Nie, S. *Science* **1998**, *281*, 2016–2018.
- (10) Kim, J.; Kim, K. S.; Jiang, G.; Kang, H.; Kim, S.; Kim, B.-S.; Park, M. H.; Hahn, S. K. *Biopolymers* **2008**, *89*, 1144–1153.
- (11) Dabbousi, B. O.; Rodriguez-Viejo, J.; Mikulec, F. V.; Heine, J. R.; Mattoussi, H.; Ober, R.; Jensen, K. F.; Bawendi, M. G. *J. Phys. Chem.* **1997**, *101*, 9463–9475.
- (12) Frantsuzov, P. A.; Marcus, R. A. *Phys. Rev. B* **2005**, *72*, 155321. 10 pp.
- (13) Louis, C.; Bazzi, R.; Marquette, C. A.; Bridot, J.-L.; Roux, S.; Ledoux, G.; Mercier, B.; Blum, L.; Perriat, P.; Tillement, O. *Chem. Mater.* **2005**, *17*, 1673–1682.
- (14) Wang, X.; Zhuang, J.; Peng, Q.; Li, Y. *Inorg. Chem.* **2006**, *45*, 6661–6665.
- (15) Doat, A.; Pellé, F.; Gardant, N.; Lebugle, A. *J. Solid State Chem.* **2004**, *177*, 1179–1187.
- (16) Beaurepaire, E.; Buissette, V.; Sauviat, M.-P.; Giaume, D.; Lahil, K.; Mercuri, A.; Casanova, D.; Huignard, A.; Martin, J.-L.; Gacoin, T. *Nano Lett.* **2004**, *4*, 2079–2083.
- (17) Konishi, T.; Yamada, M.; Soga, K.; Matsuura, D.; Nagasaki, Y. *J. Photopolym. Sci. Technol.* **2006**, *19*, 145–149.
- (18) Byrappa, K.; Devaraju, M. K.; Paramesh, J. R.; Basavalingu, B.; Soga, K. *J. Mater. Sci.* **2008**, *43*, 2229–2233.
- (19) Chang, C. A. *Invest. Radiol.* **1993**, *28*, S21–S27.
- (20) Van Wagoner, M.; Worah, D. *Invest. Radiol.* **1993**, *28*, S44–S48.
- (21) Burnett, K. R.; Wolf, G. L.; Schumacher, R.; Goldstein, E. *J. Magn. Reson. Imaging* **1985**, *3*, 65–71.
- (22) Havron, A.; Davis, M. A.; Seltzer, S. E.; Paskins-Hurlburt, A. J.; Hessel, S. J. *J. Comput. Assisted Tomogr.* **1980**, *4*, 642–648.
- (23) Carlson, C.; Hussain, S. M.; Schrand, A. M.; Braydich-Stolle, L. K.; Hess, K. L.; Jones, R. L.; Schlager, J. J. *J. Phys. Chem. B* **2008**, *112*, 13608–13619.
- (24) Yang, H.; Liu, C.; Yang, D.; Zhang, H.; Xi, Z. *J. Appl. Toxicol.* **2008**, *29*, 69–78.
- (25) Xia, T.; Kovochich, M.; Liong, M.; Mädler, L.; Gilbert, B.; Shi, H.; Yeh, J. I.; Zink, J. I.; Nel, A. E. *ACS Nano* **2008**, *2*, 2121–2134.
- (26) Hoet, P. H. M.; Brüske-Hohlfeld, I.; Salata, O. V. *J. Nanobiotechnol.* **2004**, *2*, 15 pp.
- (27) Tervonen, T.; Linkov, I.; Figueira, J. R.; Steevens, J.; Chappell, M.; Merad, M. *J. Nanopart. Res.* **2009**, *11*, 757–766.
- (28) AshaRani, P. V.; Mun, G. L. K.; Hande, M. P.; Valiyaveettill, S. *ACS Nano* **2009**, *3*, 279–290.
- (29) Nan, A.; Bai, X.; Son, S. J.; Lee, S. B.; Ghandehari, H. *Nano Lett.* **2008**, *8*, 2150–2154.
- (30) Wang, L.; O'Donoghue, M. B.; Tan, W. *Nanomedicine* **2006**, *1*, 413–426.
- (31) Mulder, W. J. M.; Griffioen, A. W.; Strijkers, G. J.; Cormode, D. P.; Nicolay, K.; Fayad, Z. A. *Nanomedicine* **2007**, *2*, 307–324.
- (32) Tyshenko, M. G.; Krewski, D. *Int. J. Nanotechnol.* **2008**, *5*, 143–160.
- (33) Oberdörster, G.; Oberdörster, E.; Oberdörster, J. *Environ. Health Persp.* **2005**, *113*, 823–839.
- (34) Geiser, M.; Rothen-Rutishauser, B.; Kapp, N.; Schürch, S.; Kreyling, W.; Schulz, H.; Semmler, M.; Im Hof, V.; Heyder, J.; Gehr, P. *Environ. Health Persp.* **2005**, *113*, 1555–1560.
- (35) Soto, K.; Garza, K. M.; Murr, L. E. *Acta Biomaterialia* **2007**, *3*, 351–358.
- (36) Moss, O. R. *Int. J. Nanotechnol.* **2008**, *5*, 3–14.
- (37) Sayes, C. M.; Warheit, D. B. *Int. J. Nanotechnol.* **2008**, *5*, 15–29.
- (38) Davoren, M.; Herzog, E.; Casey, A.; Cottineau, B.; Chambers, G.; Byrne, H. J.; Lyng, F. M. *Toxicol. in Vitro* **2007**, *21*, 438–448.
- (39) Panessa-Warren, B. J.; Warren, J. B.; Maye, M. M.; van der Lelie, D.; Gang, O.; Wong, S. S.; Ghebrehiwet, B.; Tortora, G. T.; Misewich, J. A. *Int. J. Nanotechnol.* **2008**, *5*, 55–91.
- (40) Braydich-Stolle, L.; Hussain, S.; Schlager, J. J.; Hofmann, M.-C. *Toxicol. Sci.* **2005**, *88*, 412–419.
- (41) Doiron, A. L.; Chu, K.; Ali, A.; Brannon-Peppas, L. *Proc. Natl. Acad. Sci. U.S.A.* **2008**, *105*, 17232–17237.
- (42) Heinrich, M. C.; Kuhlmann, M. K.; Kohlbacher, S.; Scheer, M.; Grgic, A.; Heckmann, M. B.; Uder, M. *Radiology* **2007**, *242*, 425–434.
- (43) Badger, D. A.; Kuester, R. K.; Sauer, J.-M.; Sipes, I. G. *Toxicology* **1997**, *121*, 143–153.
- (44) Hirano, S.; Suzuki, K. T. *Environ. Health Persp.* **1996**, *104* (1), 85–95.
- (45) McDonald, M. A.; Watkin, K. L. *Investigative Radiol.* **2003**, *38*, 305–310.
- (46) Park, J.; An, K.; Hiwang, Y.; Park, J.-G.; Noh, H.-J.; Kim, J.-Y.; Park, J.-H.; Hwang, N.-M.; Hyeon, T. *Nat. Mater.* **2004**, *3*, 891–895.
- (47) Bradley, D. C.; Chudzynska, H.; Hursthouse, M. B.; Motevali, M. *Polyhedron* **1991**, *10*, 1049–1059.
- (48) LaDuca, R. L.; Wolczanski, P. T. *Inorg. Chem.* **1992**, *31*, 1313–1315.
- (49) Peng, D.-Y.; Robinson, D. B. *Ind. Eng. Chem. Fundamen.* **1976**, *15*, 59–64.
- (50) Rajamathi, M.; Seshadri, R. *Curr. Opin. Solid State Mater. Sci.* **2002**, *6*, 337–345.
- (51) Sheldrick, G. *Acta Crystallogr. A* **2008**, *64*, 112–122.
- (52) Bronstein, L. M.; Huang, X.; Retrum, J.; Schmucker, A.; Pink, M.; Stein, B. D.; Dragnea, B. *Chem. Mater.* **2007**, *19*, 3624–3632.
- (53) Mahajan, S. V.; Dickerson, J. H. *Nanotechnology* **2007**, *18*, 325605. 6 pp.
- (54) Veith, M.; Mathur, S.; Kareiva, A.; Jilavi, M.; Zimmer, M.; Huch, V. *J. Mater. Chem.* **1999**, *9*, 3069–3079.
- (55) Gromada, J.; Montreux, A.; Chenal, T.; Ziller, J. W.; Leising, F.; Carpenter, J.-F. *Chem.—Eur. J.* **2002**, *8*, 3773–3788.
- (56) Boyle, T. J.; Bunge, S. D.; Clem, P. G.; Richardson, J.; Dawley, J. T.; M. Ottley, L. A.; Rodriguez, M. A.; Tuttle, B. A.; Avilucea, G. R.; Tissot, R. G. *Inorg. Chem.* **2005**, *44*, 1588–1600.
- (57) Du, G.; Van Tendeloo, G. *Nanotechnology* **2005**, *16*, 595–597.
- (58) Wang, X.; Li, Y. *Angew. Chem., Int. Ed.* **2002**, *41*, 4790–4793.
- (59) Wang, X.; Li, Y. *Pure Appl. Chem.* **2006**, *78*, 45–64.
- (60) Ma, L.; Chen, W.-X.; Zhao, J.; Zheng, Y.-F. *J. Cryst. Growth* **2007**, *303*, 590–596.
- (61) Tkaczyk, C.; Huk, O. L.; Mwale, F.; Antoniou, J.; Zukor, J. D.; Petit, A.; Tabrizian, M. *Biomaterials* **2009**, *30*, 460–467.
- (62) Kane, R. S.; Stroock, A. D. *Biotechnol. Prog.* **2007**, *23*, 316–319.
- (63) Gua, L.; Von Dem Bussche, A.; Buechner, M.; Yan, A.; Kane, A. B.; Hurt, R. H. *Small* **2008**, *4*, 721–727.
- (64) Grubbs, R. B. *Polym. Rev.* **2007**, *47*, 197–215.
- (65) Barrera, C.; Herrera, A. P.; Rinaldi, C. *J. Colloid Interface Sci.* **2009**, *329*, 107–113.
- (66) Hemmer, E.; Kohl, Y.; Mathur, S.; Thielecke, H.; Soga, K. *Proc. 8th Pacific Rim Conference on Ceramic and Glass Technology*, Vancouver 2009 (in press).
- (67) Nichkova, M.; Dosev, D.; Perron, R.; Gee, S. J.; Hammock, B. D.; Kennedy, I. M. *Anal. Bioanal. Chem.* **2006**, *384*, 631–637.